Tailoring coupled topological corner states in photonic crystals via symmetry breaking induced by defects

Zhaojian Zhang [*] and Junbo Yang [†]
Department of Physics, National University of Defense Technology, Changsha 410073, China

Zhihao Lan
Department of Electronic and Electrical Engineering, University College London, London WC1E 7JE, United Kingdom

(Received 6 November 2023; revised 28 January 2024; accepted 29 February 2024; published 25 March 2024)

In this paper, we present an effective approach to tailor the optical properties of coupled corner states in photonic crystal (PhC) supercell arrays by symmetry breaking. Defects are strategically introduced into unit cells to break the in-plane C_{4v} symmetry, and numerical simulations confirm the preservation of the band gap and two-dimensional Zak phases, in spite of the presence of defects. Notably, the size of defects is demonstrated to play a significant role in tuning the eigenfrequencies, quality (Q) factors, and band structures of the coupled corner states. Furthermore, these defects exhibit the ability to transform topological dark states into bright states, enabling efficient excitation by external plane waves and polarization-dependent Q factors. The resonant origin of the coupled corner states is comprehensively elucidated using a multipole decomposition analysis. This study further releases the potential of the topological light-matter interaction, holding significant implications for the design and advancement of topological photonic devices with on-demand tunability and multifrequency regions for various applications such as lasing, sensing, and quantum information processing.

DOI: 10.1103/PhysRevResearch.6.013321

I. INTRODUCTION

Recently, the field of topological physics has gained considerable attention due to its profound impact on various scientific disciplines [1,2]. Among them, topological photonics has emerged as a captivating research area exploring the interplay between topology and light [3,4]. This burgeoning field investigates the manipulation and control of light guided by topological phases, leveraging tailored structures such as photonic crystals (PhCs) and metamaterials [5,6]. These structures govern the emergence of resilient, topologically protected states of light, exemplified by topological edge and corner states, which showcase exciting phenomena including robust unidirectional waveguiding and tight localization of light [7–10]. Up to now, topological photonics has opened up a plethora of opportunities for the development of revolutionary photonic devices, including topological light sources [11,12], topological integrated photonic circuits [13,14], and topological quantum information processors [15,16].

Studying the coupling between topological states is an emerging interesting topic in topological physics [17–20]. Especially, due to the optical nature of photonic topological states, they can be evanescently coupled to each other, allowing for an expansion into an in-plane periodic configuration through PhC supercell arrays and metasurfaces [21,22]. As a result, these extended coupled topological states enable topological light formation across a larger spatial domain and demonstrate unique characteristics. For example, coupled topological corner states in PhC supercell arrays can exhibit collective behaviors [23] and surface lattice resonances [24], serving as a promising platform for light-matter interactions [25,26]. However, among the three types of coupled corner states, only coupled dipole corner states can be directly stimulated by far-field excitations, whereas the other two types, namely, coupled monopole and quadrupole corner states, remain inaccessible, which limit their potential applications for multifrequency purposes.

Meanwhile, symmetry breaking plays a crucial role in topological photonics. On the one hand, the breaking of certain symmetries, such as time-reversal symmetry and inversion symmetry, not only leads to the emergence of diverse topological phases, but also facilitates the manipulation and engineering of novel topological properties [27,28]. On the other hand, any perturbation that respects the protecting symmetries will not alter the topological invariant or destroy these topological states as long as the band gap remains open [1–3].

In this paper, we present an efficient approach to tailor the optical properties of coupled corner states in PhC supercell arrays based on the symmetry breaking. The two-dimensional (2D) Su-Schrieffer-Heeger (SSH) model is employed to propose topologically trivial and nontrivial unit cells, where defects are introduced to break the in-plane C_{4v} symmetry. Numerical simulations reveal that the band gap of the unit

[*]zhangzhaojian@nudt.edu.cn
[†]yangjunbo@nudt.edu.cn

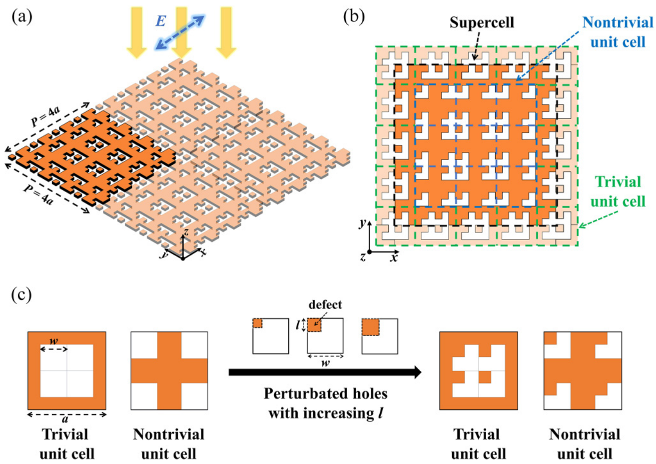

FIG. 1. (a) The geometric configuration of the supercell array with period $P = 4a$ and thickness $t = 0.5a$, where one supercell is highlighted.. For the far-field excitation, an x-polarized plane wave is incident normally from the top. (b) The top view of the supercell. Each supercell consists of a topologically nontrivial region (consisting of three rows of nontrivial unit cells) surrounded by half-layer trivial unit cells. (c) The schematics of unit cells that are perturbated by defects. Topologically trivial and nontrivial unit cells possess four compact or expanded air holes with a side length w, respectively, and each air hole is perturbated by a dielectric defect with length l at the upper-left-hand corner. The lattice constant of the unit cell is a.

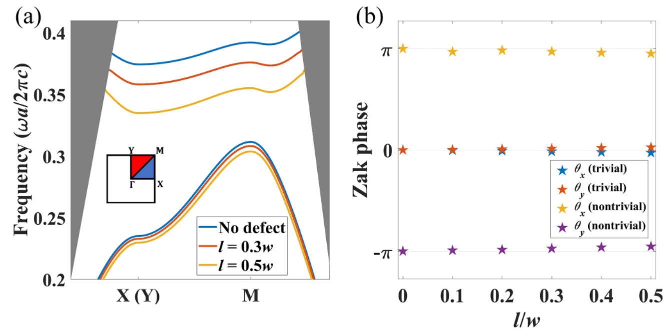

FIG. 2. (a) The band structures of nontrivial/trivial unit cells with different defect sizes. X, Y, and M denote the high-symmetry points in the momentum space. The frequencies above the light cone are shaded in gray. The inset indicates the FBZ. (b) The 2D Zak phases θ_x and θ_y of nontrivial/trivial unit cells with different defect sizes.

cells remains open despite the presence of defects, and theoretical calculations confirm the invariance of their topological properties. On this basis, PhC supercell arrays are constructed by introducing periodic nontrivial regions into trivial ones. Our findings show that the eigenfrequencies, quality (Q) factors, and band structures of coupled corner states can be effectively tuned by the size of the introduced defects. Moreover, these defects can transform coupled quadrupole and monopole corner states from dark states to bright states, allowing for efficient excitation by external plane waves, as well as a Q-factor dependency on polarization. Finally, the resonant origin of coupled corner states is elucidated via a multipole decomposition analysis. This work holds potential implications for the design and development of topological photonic devices with tunable optical responses and multifrequency regions, providing different avenues for applications in planar and quantum photonics. It should be noted that defects in this paper refer to simply added material in small areas of the unit cell to break the symmetry, which is commonly employed in the design of metasurfaces [29].

II. RESULTS AND DISCUSSION

We choose the 2D SSH model, which is the prototypical model for a second-order topological insulator (SOTI) supporting topological corner states, to lay the natural setup for the following studies. Figure 1 illustrates the geometric arrangement of the topological supercell array. The array comprises periodically arranged supercells constructed from PhC hole slab structures with a permittivity of $\varepsilon = 12$, as shown in Fig. 1(a). Each supercell consists of a square topologically nontrivial region surrounded by a trivial region as shown in Fig. 1(b). The trivial and nontrivial regions are composed of trivial and nontrivial unit cells with lattice constant a, including four compact or expanded identical air holes with $w = 0.34a$, as depicted in Fig. 1(c). Especially, a dielectric defect with length l is introduced to the upper-left-hand corner of each air hole in order to break the in-plane C_{4v} symmetry of the unit cell, as well as the supercell. Notably, each nontrivial region consists of three rows of nontrivial unit cells which are separated from each other by a row of trivial unit cells, resulting in a supercell period of $P = 4a$. According to the 2D SSH model, each supercell can be regarded as a SOTI [30].

Figure 2(a) presents the first two photonic bands of trivial and nontrivial unit cells with different sizes of defects in the first Brillouin zone (FBZ), where the second high-symmetry point is chosen at the X or Y point. The calculation is implemented via the finite-element method (FEM). Here, we only consider transverse electric (TE) modes below the light line, as the holes favor TE band gaps. Despite the perturbation of defects, the two unit cells possess identical band structures, with a band gap between the first and second bands. As the length of the defect increases from 0 to $0.5w$, the two bands slightly shift but do not close the gap, indicating the invariance of the topological properties. In addition, regardless of whether the high-symmetry point is chosen at X or Y, the band structure remains the same. Here, the topological properties of the unit cells can be distinguished by 2D Zak phases $\boldsymbol{\theta} = (\theta_x, \theta_y)$, which are defined as [30]

$$\theta_i = 2\pi P_i = \frac{1}{2\pi} \int_{\mathrm{FBZ}} dk_x dk_y \,\mathrm{Tr}[A_i(k_x, k_y)], \quad i = x, y. \quad (1)$$

Here, P_i denotes the 2D polarization, k_i is the wave vector, and $A_i = i\langle\psi(k_x, k_y)|\partial_{k_i}|\psi(k_x, k_y)\rangle$ represents the Berry connection where $|\psi(k_x, k_y)\rangle$ are the eigenmodes of bands below the band gap, which only involves the first band in this case. Due to the breaking of C_{4v} symmetry in the unit cell, the evaluation of θ_x and θ_y is not straightforward and must be calculated separately. The 2D Zak phases of unit cells with various defect sizes are calculated according to Eq. (1), as depicted in Fig. 2(b). It is observed that in the absence of defects, the trivial and nontrivial unit cells exhibit 2D Zak phases of (0,0) and (π, π), respectively (where $-\pi$ is equivalent to

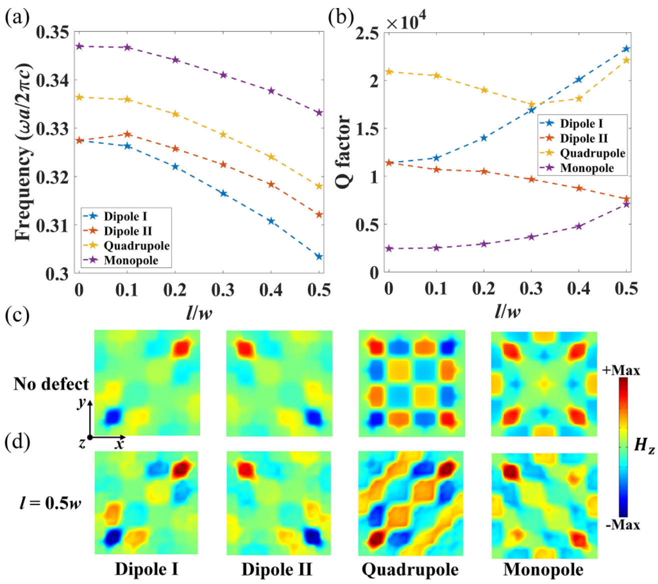

FIG. 3. (a), (b) Eigenfrequencies and Q factors of coupled corner states under different defect sizes. (c), (d) The H_z field distributions of coupled corner states in one supercell region without defects and with defects of $l = 0.5w$.

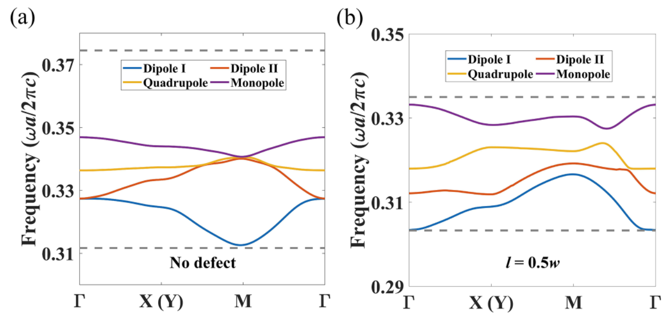

FIG. 4. Band structures of coupled corner states (a) without defects and (b) with defects of $l = 0.5w$. The gray dashed line indicates the band gap of the unit cell that makes up the supercell.

π), confirming their topologically trivial and nontrivial properties. With increasing defect size, their 2D Zak phases only exhibit slight deviations, as well as the difference between θ_x and θ_y, demonstrating that the perturbation introduced by defects does not destroy the topological properties of unit cells. Although the Zak phase may not be an appropriate topological invariant in the presence of defects, the small deviation might suggest that the major topological properties (e.g., the existence of the corner states) still persist. It is to be noted that at large l/w shown in Fig. 2(b), the Zak phases show $\theta_x = -\theta_y$ for both trivial and nontrivial unit cells, which could be explained by the reflection symmetry of the perturbed unit cell against $y = -x$ in Fig. 1(c).

While defects only introduce minor deviations to 2D Zak phases of the unit cells, they can exert a considerable influence on the optical properties of the resulting coupled corner states supported in the supercell array. In the following, we will focus on the nontrivial properties of the supercell shown in Fig. 1(b). Figure 3(a) displays the eigenmode analysis for the supercell at the Γ point, revealing the presence of four states within the band gap of the unit cell. In the absence of defects, their field distributions of the H_z component pertaining to the $x - y$ plane of the supercell at the middle of the slab ($z = t/2$) are depicted in Fig. 3(c). It is evident that the optical fields of these states are highly localized at the corners of the supercell, displaying characteristics of multipole corner states as defined by Kim *et al.* [31]. Accordingly, here they are defined as coupled dipole I, dipole II, quadrupole, and monopole corner states from low to high frequencies. The two coupled dipole corner states possess degenerate eigenfrequencies. However, the introduction of defects breaks the degeneracy of them, further resulting in a significant redshift in the eigenfrequencies of all four coupled corner states as the size of the defects increases. Simultaneously, their Q factors at the Γ point, calculated by $Q = \mathrm{Re}(\omega)/2\,\mathrm{Im}(\omega)$, also undergo pronounced changes with variations in the defect length as illustrated in Fig. 3(b). Specifically, the Q factor of the coupled monopole corner states increases with increasing defect size, while the Q factor of the coupled quadrupole corner states initially decreases and subsequently increases. Intriguingly, the Q factors of the two coupled dipole corner states exhibit opposing evolution. Figure 3(d) displays the field distributions of these states when $l = 0.5w$, highlighting the preservation of their key optical features.

We further study the impact of defects on the band structures of coupled corner states. Figure 4(a) illustrates these band structures in the FBZ of the supercell for the defect-free case, which are far beyond the light line. The bands lie within the band gap of the unit cell, and demonstrate a strong frequency dispersion due to the optical coupling effect. In addition, the band convexity indicates that the group velocity of the dipole I and monopole bands have an opposite sign compared to the dipole II and quadrupole bands. Remarkably, the presence of defects leads to significant changes in these bands, as shown in Fig. 4(b). The defects not only dramatically modify the dispersion profile of all bands, but also completely reverse the sign of the group velocity for the dipole I band, offering a promising avenue for the manipulation of band structures.

These coupled corner states lie beyond the light line of the supercell array, making them radiative and susceptible to external excitation. To further reveal the impact of defects on their radiative properties, we employ the full-wave simulation of the supercell array utilizing the finite-difference time-domain (FDTD) method, where the supercell is modeled with periodic boundary conditions in the x and y directions. According to the far-field approximation for radiation, a plane-wave source with normal incidence is introduced at the top to facilitate far-field excitation, as shown in Fig. 1(a). The transmission spectrum for the defect-free scenario is depicted in Fig. 5(a), where only a single resonant dip manifests at the eigenfrequency of the coupled dipole corner states. The field profile at the resonant frequency exhibits characteristics that validate the superposition of the two coupled dipole corner states, as illustrated in the inset of Fig. 5(a). Upon the introduction of defects, it is clearly seen that the resonant dip splits into two, signifying the breakdown of their degeneracy, consistent with the results shown in Fig. 3(a). This further confirms the simultaneous resonant excitation of the two coupled

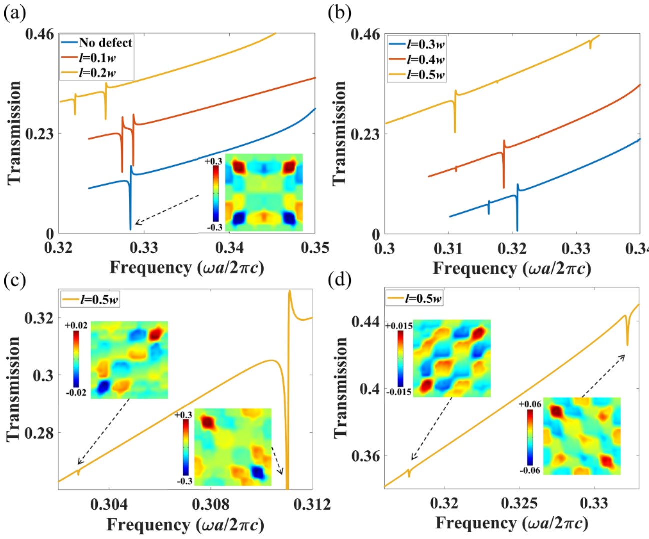

FIG. 5. (a), (b) The transmission spectra of the supercell array with various defect sizes. The inset shows the H_z field distribution of the superposed coupled dipole corner state. (c), (d) The detailed transmission spectrum of the supercell array with defect size $l = 0.5w$. The insets show the H_z field distributions of coupled dipole corner states.

dipole corner states, elucidating their nature as bright states (that is, the optical bright modes) that are directly accessible through linearly polarized light from the far field. Conversely, no spectral resonant evidence appears for the remaining two coupled corner states in Fig. 5(a), indicating their existence as dark states with finite Q factors that cannot be directly excited by linearly polarized light [32]. This nonexcitation is attributed to a complete symmetry mismatch between the states and sources, yielding a null overlap between their field profiles and incident waves.

However, introducing defects indeed breaks the in-plane C_{4v} symmetry of the supercell, thereby relaxing the symmetry protection towards coupled quadrupole and monopole corner states. As shown in Fig. 5(b), an increase in the size of defects leads to the emergence of additional resonant dips alongside the two existing ones. At $l = 0.4w$, a third resonant dip appears at the eigenfrequency of the coupled quadrupole corner states. Furthermore, at $l = 0.5w$, a fourth resonant dip emerges at the eigenfrequency of the coupled monopole corner states, and the spectral details are presented in Figs. 5(c) and 5(d). In this case, the two coupled dipole corner states are excited with distinct resonant Q factors, as confirmed by the field profiles and amplitudes shown in the insets of Fig. 5(c). Meanwhile, the field profiles at the other two resonant dips display the features of coupled quadrupole and monopole corner states, as depicted in the insets of Fig. 5(d). This further validates their simultaneous excitation. Evidently, the symmetry breaking induced by defects transforms the coupled quadrupole and monopole corner states from dark to bright states, enabling their accessibility for external excitation and offering potential benefits for practical multifrequency applications.

Due to the lack of in-plane C_{4v} symmetry in the supercell, the resonant behaviors of coupled corner states exhibit a sensitivity to the polarization of the incident plane wave. As presented in Fig. 6, the transmission spectra at $l = 0.5w$ vary under different polarization angles ϕ. It is shown that the resonant Q factors of these states can be effectively tuned by adjusting the polarization direction. For instance, as shown in Fig. 6(a), when the polarization angle is tuned from 0° to 45°, the excitation of the coupled dipole I corner state is completely quenched, while the resonant Q factor of the coupled dipole II corner state is gradually enhanced from 4800 to 4950, which is calculated by fitting the Fano formula. Similarly, increasing the polarization angle also results in higher resonant Q factors for the coupled quadrupole and monopole states, as depicted in Fig. 6(b). This tunability arises from the fact that tuning the polarization direction actually modifies the symmetry match between the states and sources, thereby altering the accessibility of the radiative channel and subsequently leading to changes in the radiative loss of these resonances.

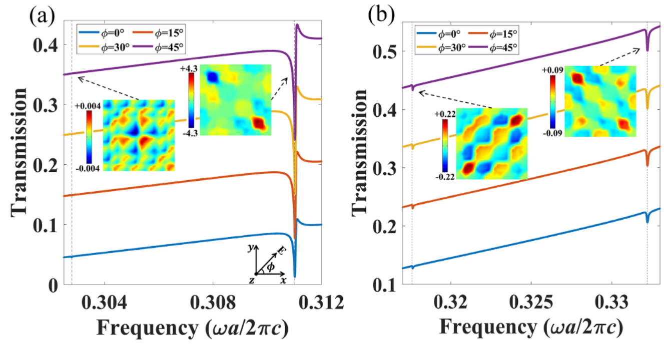

FIG. 6. The transmission spectra of the supercell array with defect size $l = 0.5w$ under the plane-wave excitation with various polarization angles ϕ defined in the inset. The insets also show the H_z field distributions of coupled corner states. (a) and (b) show spectra in different frequency regions.

Finally, to gain deeper physical insights into the resonant origin of coupled corner states supported in the dielectric medium, we implement the electromagnetic multipole expansion in the Cartesian coordinate system, and the leaky nature of these states allows us to decompose their far-field scattering cross sections C_{sca} into several components as follows [33,34]:

$$\begin{aligned} C_{\mathrm{sca}} &= C_{\mathrm{sca}}^{p} + C_{\mathrm{sca}}^{T} + C_{\mathrm{sca}}^{m} + C_{\mathrm{sca}}^{Q^e} + C_{\mathrm{sca}}^{Q^m} + \cdots \\ &= \frac{k^4}{6\pi\varepsilon_0^2|\mathbf{E}_0|^2}\left[\sum_{\alpha}\left(|p_\alpha + ikT_\alpha|^2 + \frac{|m_\alpha|^2}{c}\right)\right. \\ &\quad \left. + \frac{1}{120}\sum_{\alpha\beta}\left(\left|kQ_{\alpha\beta}^{e}\right|^2 + \left|\frac{kQ_{\alpha\beta}^{m}}{c}\right|^2\right) + \cdots\right]. \end{aligned} \tag{2}$$

Here, p_α, T_α, and m_α denote the electric dipole (ED), toroidal dipole (TD), and magnetic dipole (MD) moments, respectively. Additionally, $Q_{\alpha\beta}^{e}$ and $Q_{\alpha\beta}^{m}$ indicate electric quadrupole (EQ) and magnetic quadrupole (MQ) moments, correspondingly. $\mathbf{E}_0$ denotes the electric field amplitude of the input plane wave, while k represents the wave number. ε_0 signifies the vacuum permittivity, c represents the speed of light, and $\alpha, \beta = x, y, z$.

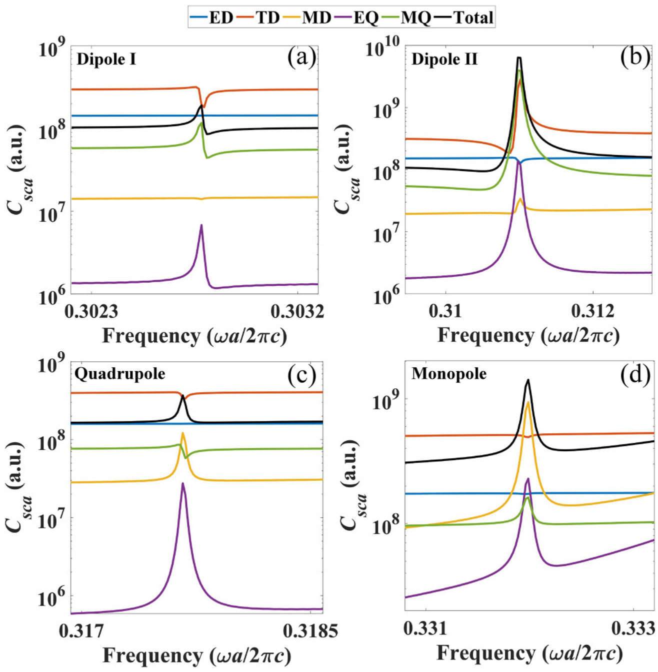

FIG. 7. Multipole scattering cross sections of coupled corner states with defects of $l = 0.5w$.

The decomposed scattering cross sections of these states at $l = 0.5w$ are presented in Fig. 7. It is shown that the resonant response, namely, the resonant dip, of the two coupled dipole corner states is dominated by the TD and MQ, where the ED is the radiative background from the nonresonant light source. To understand the origin of these multipoles, the H_z distribution and displacement current density (denoted by red arrows) of the coupled dipole I corner state are illustrated in Fig. 8(a). The magnetic fields localized at the corners create a pair of MDs with opposite phases, giving rise to the MQ. Concurrently, the displacement currents circulate counterclockwise around the upper-right-hand corner and clockwise nearby. Examining the $x - z$ cross section of the structure in Fig. 8(b), magnetic field vectors (denoted by blue arrows) reveal a closed magnetic vortex passing through the current loops, which characterizes the TD and also exist at the bottom-left-hand corner. A similar multipole origin applies to the coupled dipole II corner state. However, for the coupled quadrupole state, as shown in Fig. 7(c), the contribution of the MQ diminishes, while the MD increases. This occurs because the MDs with negative phases are weakened, disrupting the balance of the MQ. Similarly, for the coupled monopole corner state, as depicted in Fig. 7(d), the MD becomes the dominant contribution, followed by the TD. The MQ breaks down in this case since the MDs at all corners have the same phase. The multipole expansion demonstrates the inherent multipole nature of coupled corner states and opens up possibilities for manipulating these states through multipole engineering. This manipulation has the potential to enrich their optical properties, enabling intriguing phenomena such as nonradiative anapole characteristics and unidirectional emission [35]. These intriguing possibilities warrant further exploration in future studies.

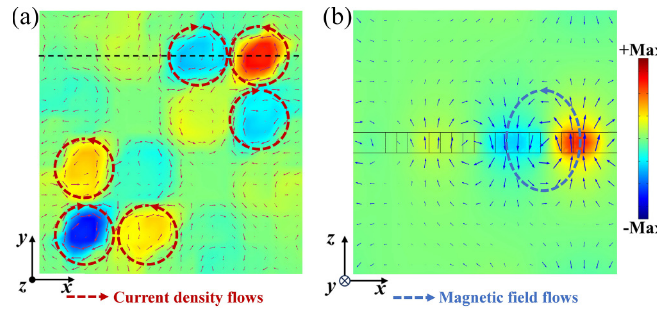

FIG. 8. (a) The H_z field distribution and displacement current density (indicated by red arrows) of the coupled dipole I corner state. (b) The H_z field distribution and magnetic field vectors (indicated by blue arrows) of the coupled dipole I corner state. The position of the $x - z$ cross section is indicated by the black dashed line in Fig. 8(a).

III. CONCLUSION

In conclusion, this paper presents a symmetry-breaking approach to manipulate the optical properties of coupled corner states in PhC supercell arrays, with promising implications for the design of topological photonic devices. By utilizing the 2D SSH model and introducing defects to break the in-plane C_{4v} symmetry, we demonstrate through simulations that the unit cells maintain an open band gap and nearly invariant 2D Zak phases. Our findings highlight the tunability of eigenfrequencies, Q factors, and band structures of coupled corner states by adjusting the defect size. Moreover, these defects enable the transformation of dark states to bright states, enhancing excitation efficiency and polarization-dependent Q factors. The resonant origin of coupled corner states is further elucidated through a multipole decomposition analysis. This study further unleashes the potential of the interaction between topological light and matter, and opens exciting possibilities for the realization of on-demand tunable and multifrequency topological devices in various photonic applications including sensing, lasing, and quantum information processing.

ACKNOWLEDGMENTS

The work is supported by the National Key Research and Development Program of China (Grant No. 2022YFF0706005), the National Natural Science Foundation of China (Grants No. 62305387, No. 62275271, No. 12272407, and No. 62275269), the Natural Science Foundation of Hunan Province (Grants No. 2023JJ40683, No. 2022JJ40552, and No. 2020JJ5646), and the Foundation of NUDT (ZK23-03).

[1] M. Z. Hasan and C. L. Kane, Colloquium: Topological insulators, Rev. Mod. Phys. **82**, 3045 (2010).

[2] X.-L. Qi and S.-C. Zhang, Topological insulators and superconductors, Rev. Mod. Phys. **83**, 1057 (2011).

[3] T. Ozawa, H. M. Price, A. Amo, N. Goldman, M. Hafezi, L. Lu, M. C. Rechtsman, D. Schuster, J. Simon, O. Zilberberg *et al.*, Topological photonics, Rev. Mod. Phys. **91**, 015006 (2019).

[4] Z. Lan, M. L. Chen, F. Gao, S. Zhang, and E. Wei, A brief review of topological photonics in one, two, and three dimensions, Rev. Phys. **9**, 100076 (2022).

[5] G.-J. Tang, X.-T. He, F.-L. Shi, J.-W. Liu, X.-D. Chen, and J.-W. Dong, Topological photonic crystals: Physics, designs, and applications, Laser Photonics Rev. **16**, 2100300 (2022).

[6] S. Ma, B. Yang, and S. Zhang, Topological photonics in metamaterials, Photonics Insights **1**, R02 (2022).

[7] Z. Wang, Y. Chong, J. D. Joannopoulos, and M. Soljačić, Observation of unidirectional backscattering-immune topological electromagnetic states, Nature (London) **461**, 772 (2009).

[8] Y. Yang, Y. F. Xu, T. Xu, H.-X. Wang, J.-H. Jiang, X. Hu, and Z. H. Hang, Visualization of a unidirectional electromagnetic waveguide using topological photonic crystals made of dielectric materials, Phys. Rev. Lett. **120**, 217401 (2018).

[9] Y. Ota, F. Liu, R. Katsumi, K. Watanabe, K. Wakabayashi, Y. Arakawa, and S. Iwamoto, Photonic crystal nanocavity based on a topological corner state, Optica **6**, 786 (2019).

[10] B.-Y. Xie, G.-X. Su, H.-F. Wang, H. Su, X.-P. Shen, P. Zhan, M.-H. Lu, Z.-L. Wang, and Y.-F. Chen, Visualization of higher-order topological insulating phases in two-dimensional dielectric photonic crystals, Phys. Rev. Lett. **122**, 233903 (2019).

[11] M. A. Bandres, S. Wittek, G. Harari, M. Parto, J. Ren, M. Segev, D. N. Christodoulides, and M. Khajavikhan, Topological insulator laser: Experiments, Science **359**, eaar4005 (2018).

[12] Y. Zeng, U. Chattopadhyay, B. Zhu, B. Qiang, J. Li, Y. Jin, L. Li, A. G. Davies, E. H. Linfield, B. Zhang *et al.*, Electrically pumped topological laser with valley edge modes, Nature (London) **578**, 246 (2020).

[13] X.-T. He, E.-T. Liang, J.-J. Yuan, H.-Y. Qiu, X.-D. Chen, F.-L. Zhao, and J.-W. Dong, A silicon-on-insulator slab for topological valley transport, Nat. Commun. **10**, 872 (2019).

[14] M. I. Shalaev, W. Walasik, A. Tsukernik, Y. Xu, and N. M. Litchinitser, Robust topologically protected transport in photonic crystals at telecommunication wavelengths, Nat. Nanotechnol. **14**, 31 (2019).

[15] S. Barik, A. Karasahin, C. Flower, T. Cai, H. Miyake, W. DeGottardi, M. Hafezi, and E. Waks, A topological quantum optics interface, Science **359**, 666 (2018).

[16] Y. Chen, X.-T. He, Y.-J. Cheng, H.-Y. Qiu, L.-T. Feng, M. Zhang, D.-X. Dai, G.-C. Guo, J.-W. Dong, and X.-F. Ren, Topologically protected valley-dependent quantum photonic circuits, Phys. Rev. Lett. **126**, 230503 (2021).

[17] I. Belopolski, S.-Y. Xu, N. Koirala, C. Liu, G. Bian, V. N. Strocov, G. Chang, M. Neupane, N. Alidoust, D. Sanchez *et al.*, A novel artificial condensed matter lattice and a new platform for one-dimensional topological phases, Sci. Adv. **3**, e1501692 (2017).

[18] J. Strunz, J. Wiedenmann, C. Fleckenstein, L. Lunczer, W. Beugeling, V. L. Müller, P. Shekhar, N. T. Ziani, S. Shamim, J. Kleinlein *et al.*, Interacting topological edge channels, Nat. Phys. **16**, 83 (2020).

[19] J. Chen, W. Liang, and Z.-Y. Li, Strong coupling of topological edge states enabling group-dispersionless slow light in magneto-optical photonic crystals, Phys. Rev. B **99**, 014103 (2019).

[20] L. Yu, H. Xue, and B. Zhang, Topological slow light via coupling chiral edge modes with flatbands, Appl. Phys. Lett. **118**, 071102 (2021).

[21] Z. Zhang, J. You, Z. Lan, and N. Panoiu, Lattice topological edge and corner modes of photonic crystal slabs, J. Opt. **23**, 095102 (2021).

[22] Z. Gu, J. Chen, B. Gao, W. Wu, Z. Zhao, W. Cai, X. Zhang, M. Ren, and J. Xu, Metasurfaces with high-Q resonances governed by topological edge state, Opt. Lett. **47**, 1822 (2022).

[23] Z. Zhang, J. Yang, T. Du, H. Ma, and X. Jiang, Collective topological corner modes in all-dielectric photonic crystal supercell arrays, Opt. Lett. **47**, 1642 (2022).

[24] Z. Zhang, Z. Lan, H. Chen, Y. Yu, and J. Yang, Tailoring topological corner states in photonic crystals by near-and far-field coupling effects, Chin. Phys. B **32**, 124201 (2023).

[25] Z. Zhang, J. Yang, T. Du, and X. Jiang, Topological multipolar corner state in a supercell metasurface and its interplay with two-dimensional materials, Photonics Res. **10**, 855 (2022).

[26] Z. Gu, H. Tan, J. Peng, J. Chen, D. Zhang, F. Xie, W. Wu, W. Cai, M. Ren, and J. Xu, Electro-optic modulation using lithium niobate metasurfaces with topological corner state, Appl. Phys. Lett. **122**, 171706 (2023).

[27] C.-K. Chiu, J. C. Y. Teo, A. P. Schnyder, and S. Ryu, Classification of topological quantum matter with symmetries, Rev. Mod. Phys. **88**, 035005 (2016).

[28] Y. Ota, K. Takata, T. Ozawa, A. Amo, Z. Jia, B. Kante, M. Notomi, Y. Arakawa, and S. Iwamoto, Active topological photonics, Nanophotonics **9**, 547 (2020).

[29] Z. Liu, Y. Xu, Y. Lin, J. Xiang, T. Feng, Q. Cao, J. Li, S. Lan, and J. Liu, High-Q quasibound states in the continuum for nonlinear metasurfaces, Phys. Rev. Lett. **123**, 253901 (2019).

[30] B.-Y. Xie, H.-F. Wang, H.-X. Wang, X.-Y. Zhu, J.-H. Jiang, M.-H. Lu, and Y.-F. Chen, Second-order photonic topological insulator with corner states, Phys. Rev. B **98**, 205147 (2018).

[31] H.-R. Kim, M.-S. Hwang, D. Smirnova, K.-Y. Jeong, Y. Kivshar, and H.-G. Park, Multipolar lasing modes from topological corner states, Nat. Commun. **11**, 5758 (2020).

[32] D. Gómez, Z. Teo, M. Altissimo, T. Davis, S. Earl, and A. Roberts, The dark side of plasmonics, Nano Lett. **13**, 3722 (2013).

[33] R. Alaee, C. Rockstuhl, and I. Fernandez-Corbaton, An electromagnetic multipole expansion beyond the long-wavelength approximation, Opt. Commun. **407**, 17 (2018).

[34] T. Hinamoto and M. Fujii, MENP: an open-source MATLAB implementation of multipole expansion for nanophotonics, OSA Contin. **4**, 1640 (2021).

[35] T. Liu, R. Xu, P. Yu, Z. Wang, and J. Takahara, Multipole and multimode engineering in Mie resonance-based metastructures, Nanophotonics **9**, 1115 (2020).